Effect of magnetic nanoparticles on magnetic field homogeneity

Si-Lin Guo(郭斯琳)[1,2,†], Wen-Tong Yi(易文通)[3], and Zhuang-Zhuang Li(李壮壮)[3]

[1] *Laboratory of Science and Technology on Integrated Logistics Support, National University of Defense Technology, Changsha* 410073, *China*
[2] *College of Intelligence Science and Technology, National University of Defense Technology, Changsha* 410073, *China*
[3] *School of Artificial Intelligence and Automation, Huazhong University of Science and Technology, Wuhan* 430074, *China*

(Received 27 July 2022; revised manuscript received 4 December 2022; accepted manuscript online 9 December 2022)

The mechanism of magnetic nanoparticles (MNPs) affecting magnetic field uniformity is studied in this work. The spatial distribution of MNPs in liquid is simulated based on Monte Carlo method. The induced field of the single MNP is combined with the magnetic field distribution of magnetofluid. In the simulation, magnetic field uniformity is described by a statistical distribution. As the chemical shift (CS) and full width at half maximum (FWHM) of magnetic resonance (MR) spectrum can reflect the uniformity of magnetic field, the simulation is verified by spectrum experiment. Simulation and measurement results prove that the CS and FWHM of the MR spectrum are basically positively correlated with the concentration of MNPs and negatively correlated with the temperature. The research results can explain how MNPs play a role in MR by affecting the uniform magnetic field, which is of great significance in improving the temperature measurement accuracy of magnetic nanothermometers and the spatial resolution of magnetic particle imaging.

Keywords: magnetic nanoparticle, field distribution, Monte Carlo method

PACS: 02.70.Uu, 07.55.Db **DOI:** 10.1088/1674-1056/acaa26

1. Introduction

The treatment effect and safety of tumor hyperthermia largely depend on the accurate *in-vivo* temperature measurement and temperature imaging. Because magnetic resonance imaging (MRI) can be used for non-invasively measuring temperature and temperature changes deep inside the living body, tumor hyperthermia guided by MRI is the research focus of clinical tumor physical therapy.[1] The key of magnetic resonance (MR) thermometry is the temperature sensitivity of hydrogen nuclear magnetic resonance parameters such as proton resonance frequency (PRF) shift, T1, T2, and diffusion. However, owing to the low inherent temperature sensitivity of these parameters limiting the improvement of temperature measurement performance, the temperature resolution of MR thermometry has been 1 °C for many years.[2]

The using of temperature-sensitive contrast agents provides a new exploration direction for alleviating the limitation to temperature resolution. Contrast agents improve the temperature sensitivity of MR parameters with the temperature sensitivity of its magnetization. Hankiewicz *et al.* used Gd particles and $Co_{0.3}Zn_{0.7}Fe_2O_4$ clusters in MR via nuclear magnetic resonance (NMR) linewidth to determine temperature changes with an accuracy of ±1.0 °C.[3,4] Zhang *et al.* studied the effect of the magnetization response of superparamagnetic iron oxide nanoparticles (SPIONs) on R2 relaxation rate and used SPIONs as temperature sensors with a temperature estimation accuracy of about 0.05 °C.[5] Guo *et al.* proposed an MR temperature measurement method with an accuracy of 0.1 °C based on the influence of the magnetization of SPIONs on chemical shift.[6]

In the above researches, the nanoparticles with unique superparamagnetism contained in the contrast agents can be collectively referred to as magnetic nanoparticles (MNPs). Owing to their small size and physicochemical properties, MNPs have widespread applications in biotechnology and biomedical areas, such as cell label,[7] drug targeted release,[8] tumor magnetic thermal,[9,10] and magnetic resonance imaging (MRI).[11–13] As the temperature sensitivity of magnetic susceptibility, MNPs also can be used as the temperature sensor to realize the remote temperature measurement.[14–18]

In practical applications, MNPs are usually evenly distributed in liquid to form magnetofluid. When the magnetofluid is under a uniform magnetic field, the induced field generated by MNPs can influence the field homogeneity. From the perspective of the magnetofluid system as a whole, magnetization can be described by Langevin equation.[19] However, MR is a quantum mechanical resonant effect. In order to study the influence of MNPs on MR more accurately, it is necessary to analyze the effect of magnetofluid on the magnetic field from the perspective of particles.

The mechanism of MNPs affecting magnetic field uniformity is studied in this work. Based on the magnetic dipole theory, the induced magnetic field of MNPs is calculated. Combining with the particle distribution in magnetic fluid, which is simulated by Monto Carlo method, the influence of MNPs on the homogeneity of the static magnetic field is calculated. The influence of MNPs' characteristics, such as concentration and temperature, on magnetic field homogeneity is analyzed with

†Corresponding author. E-mail: silin7069@qq.com

© 2023 Chinese Physical Society and IOP Publishing Ltd

the simulation results and the experimental results.

2. Model and theory

For the magnetofluid placed in a uniform magnetic field, the following assumptions are made on the basis that MNPs are single-domain: (i) only magnetic interaction and thermodynamic motion are dominant in the interaction between particles; (ii) the liquid sample is large enough to ensure the action of particles is within the sample range; (iii) particles are randomly distributed in the liquid.

2.1. Induced field of single magnetic particle

As the superposition principle states that the fields created by different sources, as vectors, can be added together, the magnetization of magnetofluid can be seen as the induced fields produced by each particle added together. To the nanoscale particles, each particle is regarded as a magnetic dipole, then the dipole is modeled as a uniformly magnetized spherical sphere.[20,21] as shown in Fig. 1. Considering the particle as a sphere of radius R, the magnetic permeability outside the sphere is μ_1, the magnetic permeability inside the sphere is μ_2.

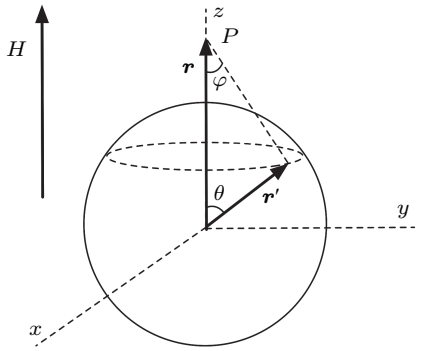


Fig. 1. Schematic diagram of magnetic dipole in magnetic field.

The vector potential produced by the dipole at a point P of radius vector $\boldsymbol{r}$ can be calculated as a sum of contributions of all volume elements of radius vector $\boldsymbol{r}'$. One can see from Fig. 1 that $r' = \sqrt{r^2 + R^2 - 2rR\cos\theta}$. In accordance with the vector analysis, the volume integral can be transformed into an integral over the surface of the sphere. The magnetic dipole moment $\boldsymbol{m}$, which is parallel to the direction of magnetic field $\boldsymbol{H}$, can be obtained to be[22]

$$\boldsymbol{m} = \frac{4\pi\mu_1(\mu_2-\mu_1)R^3}{2\mu_1+\mu_2}\boldsymbol{H}. \tag{1}$$

The external magnetic field $\boldsymbol{H}_{\text{ext}}$ and the internal field $\boldsymbol{H}_{\text{int}}$ of the sphere can be written as[21,23]

$$\begin{cases} \boldsymbol{H}_{\text{ext}} = \text{H} + \dfrac{1}{4\pi\mu_1}\left[\dfrac{3(\boldsymbol{m}\cdot\boldsymbol{r})\boldsymbol{r}}{r^5} - \dfrac{\boldsymbol{m}}{r^3}\right], \\ \boldsymbol{H}_{\text{int}} = \dfrac{3\mu_1}{2\mu_1+\mu_2}\boldsymbol{H}. \end{cases} \tag{2}$$

Based on Eq. (2) and the superposition principle of the magnetic field, the field distributions of MNPs with 10-nm diameter at 50-mT field are simulated, and the results are shown in Fig. 2.

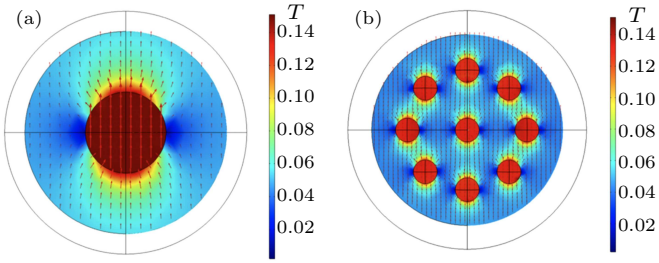


Fig. 2. Magnetic field distribution of (a) single particle and (b) multiple particles with fixed position.

2.2. Distribution of magnetic particles

In the actual situation, MNPs do not stay in position as shown in Fig. 2(b). The particle distribution is randomly determined by the energy. In addition to the external magnetic field, MNPs also receive the interaction between particles, the repulsion caused by particle coating, and the Van der Waals force, which all affect the thermodynamic motion and distribution of particles.[24] Therefore, Monte Carlo method is selected to simulate the particle distribution.[25]

It is assumed that there are N particles are distributed homogeneously in a cube with the side length L. The particle size is D and the coating thickness is δ. The state of each particle is (x_i, y_i, z_i, β_i), where (x_i, y_i, z_i) is the position and β_i is the angle between magnetic field $\boldsymbol{H}$ and magnetic moment $\boldsymbol{m}$.

The order of the Van der Waals energy can be equivalent to the thermodynamic energy, so it cannot be ignored. The Van der Waals energy E_{v} can be written as[26]

$$E_{vi} = -k_{\text{B}}T\lambda_{\text{v}}\sum_{j\neq i}\left[\frac{2}{s^2-4} + \frac{2}{s^2} + \ln\left(\frac{s^2-4}{s^2}\right)\right], \tag{3}$$

where $\lambda_{\text{v}} = A/(4k_{\text{B}}T)$, $s = \frac{2(|\boldsymbol{R}_{ij}|-D-2\delta)}{D}+1$, $\boldsymbol{R}_{ij}$ is the vector from particle i to particle j, $1.5D+2\delta < |\boldsymbol{R}_{ij}| \leq 10D$, T is the absolute temperature, Boltzmann constant $k_{\text{B}} = 1.3806505 \times 10^{-23}$ J/K, and Hamaker constant $A = 10^{-19}$ J.

When the distance between particles is $|\boldsymbol{R}_{ij}| \leq D+2\delta$, the particle coating will produce resistance energy E_{s}, which can be calculated from[27]

$$E_{si} = k_{\text{B}}T\lambda_{\text{s}}\sum_{j\neq i}\left[2 - \frac{l+2}{t}\ln\left(\frac{1+t}{1+\frac{l}{2}}\right) - \frac{l}{t}\right], \tag{4}$$

where $\lambda_{\text{s}} = \pi D^2 N'/2$, $l = 2(|\boldsymbol{R}_{ij}|-D)/D$, $t = 2\delta/D$, and N' is the number of surfactant molecules per unit surface area.

Based on the magnetic dipole–dipole interaction, the interaction energy of particles E_{d} can be written as[22]

$$E_{\text{di}} = (k_{\text{B}}T\cdot\lambda_{\text{d}})\sum_{j\neq i}\left(\frac{D}{R_{ij}}\right)^3$$

$$\times(\boldsymbol{n}_i\cdot\boldsymbol{n}_j-3(\boldsymbol{n}_i\cdot\boldsymbol{r}_{ij})(\boldsymbol{n}_j\cdot\boldsymbol{r}_{ij})), \tag{5}$$

where $\lambda_{\rm d}=\mu_0 m^2/(4\pi D^3 k_{\rm B}T)$, the permeability of vacuum $\mu_0=4\pi\times10^{-7}$ H/m, $\boldsymbol{r}_{ij}$ is the vector drawn from particle i to j, $\boldsymbol{n}_i$ and $\boldsymbol{n}_j$ are the unit vectors of magnetic moments.

The magnetostatic energy $E_{\rm h}$ can be calculated from[27]

$$E_{{\rm h}i}=-\mu_0 mH\cos\beta_i=-k_{\rm B}T\xi\cos\beta_i. \tag{6}$$

Therefore, the system energy of one state can be written as

$$E=\sum_{i=1}^{N}(E_{{\rm d}i}+E_{{\rm v}i}+E_{{\rm s}i}+E_{{\rm h}i}). \tag{7}$$

For each state, particles have random movement and reach a new position:

$$\begin{cases} x_i'=x_i+S_{\max}(2\times{\rm rand}-1),\\ y_i'=y_i+S_{\max}(2\times{\rm rand}-1),\\ z_i'=z_i+S_{\max}(2\times{\rm rand}-1),\\ \beta_i'=\beta_i+S_{\beta\max}(2\times{\rm rand}-1), \end{cases} \tag{8}$$

where $S_{\max}$ is the maximum displacement value of MNPs and $S_{\beta\max}$ is the maximum rotation angle of the magnetic moment.

Based on the Metropolis algorithm, the position of MNPs is simulated by Monte Carlo method. Let ΔE be the change of system energy turning from an old state $x(n)$ into a new state $x(n+1)$, then the probability of acceptance p will be[25]

$$p=\min\left\{1,\exp\left(-\frac{\Delta E}{k_{\rm B}T}\right)\right\}, \tag{9}$$

where $\Delta E=E(n+1)-E(n)$. If the system energy decreases ($\Delta E<0$), the new state can be accepted and MNPs can move. If the energy remains unchanged or increases, it means that the system deviating from the most probable position, and then the state change will be judged by the algorithm. The system will generate a random number between 0 and 1. If the number is less than the probability p, the system change will be accepted, otherwise, the transfer will be rejected and wait for the next state change.

So, the simulation of the effect of magnetofluid on a magnetic field is composed of three main steps: The MNP distribution is randomly simulated with the energy constraint.

(I) the magnetic field intensity of magnetofluid is obtained by superimposing the induced magnetic field produced by each particle with the external magnetic field.

(II) The spatial distribution of the magnetic field is obtained by calculating the probability distribution of the magnetic field intensity of each point in the simulation space.

3. Results and discussion

3.1. Simulation results

The parameters in the particle system, used in the simulation, are as follows: the number N of particles is 100, the diameter D is 5 nm, the particle coating thickness is $\delta=0.15D$ and the saturation magnetization is $M_{\rm s}=4.414\times10^5$ A/m. The external magnetic field strength is $B_0=\mu_0 H_0=50$ mT. The temperature is $T_0=300$ K. $N'=10^{18}/{\rm m}^2$, $S_{\max}=0.25D$, and $S_{\beta\max}=\pi/18$. Considering the simulation capability of the computer, the space step is set to $0.2D$.

For the particles at the edge of the simulation space, the magnetic field lines that are not included in the simulation space also have a significant influence on the overall magnetic field. Because the simulation space cannot be expanded indefinitely, the simulation space is expanded while the particles are restricted to randomly walk in a certain activity space to avoid the influence of the particles at the edge.

The simulation results about the spatial distribution of MNPs and the probability distribution of magnetic field intensity are shown in Fig. 3. The simulation results clearly reflect the influence of MNPs on the magnetic field distribution, including the offset of the distribution center and the increase of the full width at half maximum (FWHM) of the distribution curve. Because the order of magnitude of the influence is small relative to the external magnetic field intensity, it is described by one part per million (ppm).

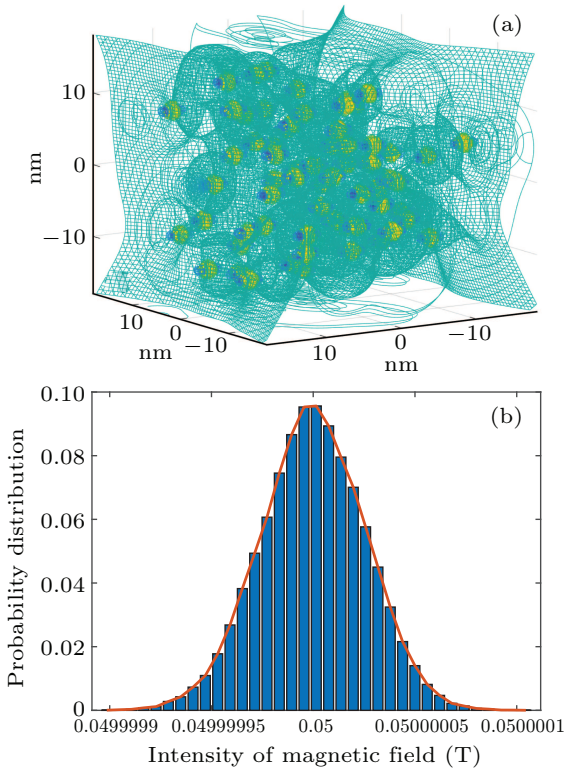


Fig. 3. (a) Spatial distribution of MNPs and (b) probability distribution of magnetic field intensity.

Because the particle core size, concentration and temperature directly affect the magnetic moment and thermal motion of MNPs, the simulation results of particle diameter and concentration dependence of the distribution of the magnetic field are shown in Figs. 4 and 5. The simulation temperature ranges

from 290 K to 320 K, which is determined by the magnetic hyperthermia temperature range. The simulation results of temperature dependence are shown in Fig. 6.

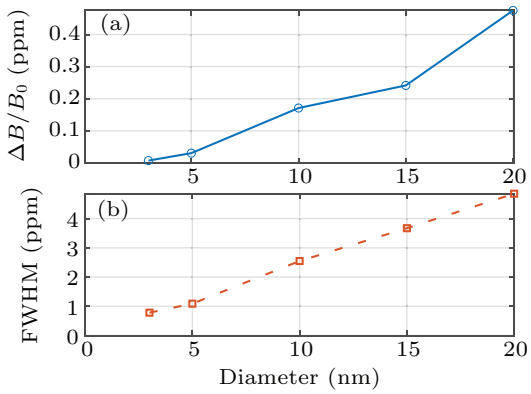


Fig. 4. Simulation results of particle diameter dependence of (a) offset of magnetic field intensity and (b) FWHM of probability distribution.

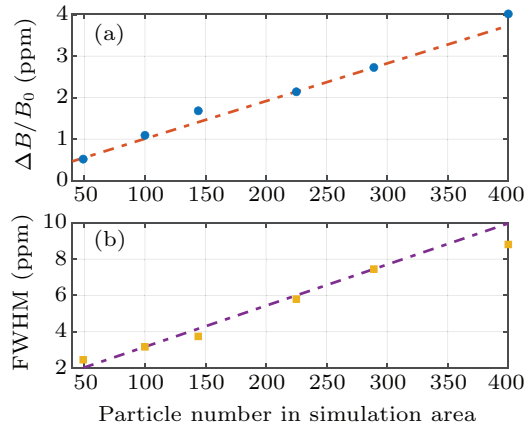


Fig. 5. Simulation results of particle concentration dependence of (a) offset of magnetic field intensity and (b) FWHM of probability distribution, with particle diameter being 5 nm.

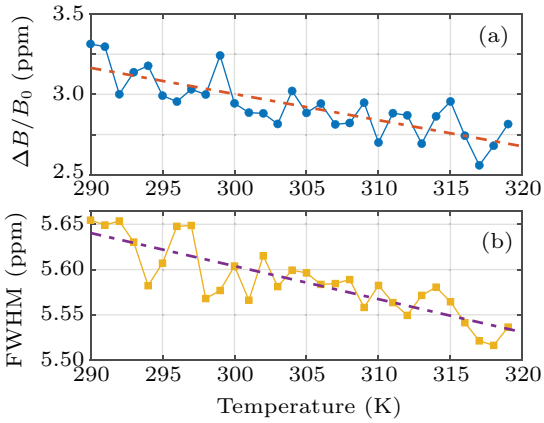


Fig. 6. Simulation results of temperature dependence of (a) offset of magnetic field intensity and (b) FWHM of probability distribution, with particle diameter being 5 nm.

The simulation results show that with the increase of particle size and concentration, the inhomogeneity of the magnetic field increases, which is consistent with the actual situation. When particle size and concentration are specified, the magnetic field inhomogeneity decreases with the increase of temperature. This is consistent with the description in the MNP temperature measurement that the induced magnetization of MNPs decreases with the increase of temperature.[18] The reason why the simulation results fluctuate obviously is the influence of particle motion. The higher the temperature, the more intense the thermal motion will be. Equations (6)–(9) show the scenarios of influence of temperature on the Hamiltonian of the particle system. The particle motion intensifies, which means that the particle position is more random in the result, resulting in a greater difference in the distribution of the magnetic field.

3.2. Experimental results

In order to verify the simulations, experiments are carried out by using MR spectroscopy.

The NMR spectroscopy is the preeminent technique for determining the structure of organic compounds.[28] As the electrons surrounding the proton are charged particles, they move in response to the external magnetic field $B = \mu_0 H$, thereby generating a secondary field. This secondary field shields the nucleus from the applied field, which makes the proton nuclei in different compounds behave differently in NMR.[29] As the NMR frequency is dependent on magnetic field , the induced field of MNPs can be reflected by the change of chemical shift.

In the experiments, heavy water Aldrich-450510 (Sigma-Aldrich, Germany) with tetramethylsilane (TMS) is used to dilute the iron concentration. The NMR spectrum measurements are performed at the 1-T system Spinsolve 43 (Magritek, New Zealand). 400 µl of experimental reagents are stored in 5-mm diameter NMR tubes (NORELL, US). The spectra for heavy water and MNP reagents with different concentrations are shown in Fig. 7. The properties and test results of reagents are listed in Table 1.

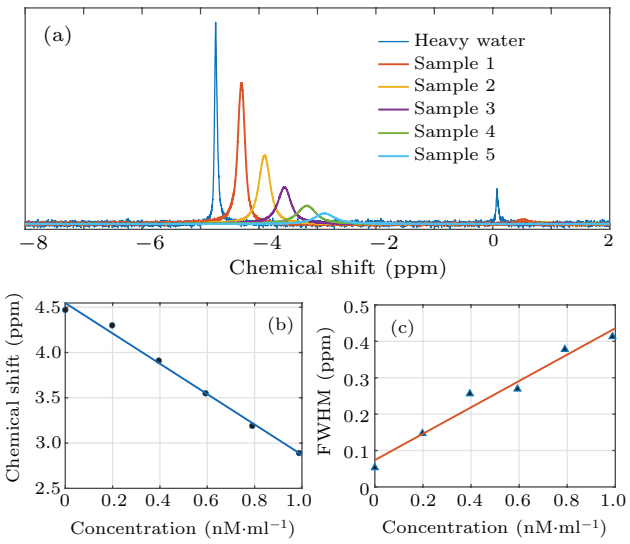


Fig. 7. (a) The 43-MHz 1-H NMR spectra *versus* chemical shift for different samples, (b) chemical shift *versus* concentration, and (c) FWHM *versus* concentration.

Table 1. Properties and experimental results of reagents.

Sample	Molar concentration (nM/ml)	Chemical shift (ppm)	FWHM (ppm)
Heavy water	0	4.47	0.053
1	0.198	4.30	0.147
2	0.395	3.91	0.256
3	0.593	3.55	0.269
4	0.79	3.19	0.378
5	0.988	2.89	0.413

The experimental results show that the peak of heavy water is shifted and widened obviously with the increase of MNP reagent concentration, which proves that the simulation results are consistent with the reality. In NMR, magnetic nanoparticles alter the resonance frequency of water molecules by affecting the uniformity of the magnetic field, and this change can be clearly reflected in the spectrum.

The results of the temperature experiment are shown in Fig. 8. As the chemical shift of heavy water itself also changes with temperature,[30,31] the shift change produced by MNPs has been calculated as shown in Fig. 8(b). Experimental results show that both chemical shift and FWHM decrease with the increase of temperature, which is consistent with the simulation results. In addition to the influence of experimental results caused by particle motion, another reason is that the temperature rise increases the measurement noise of NMR spectra.

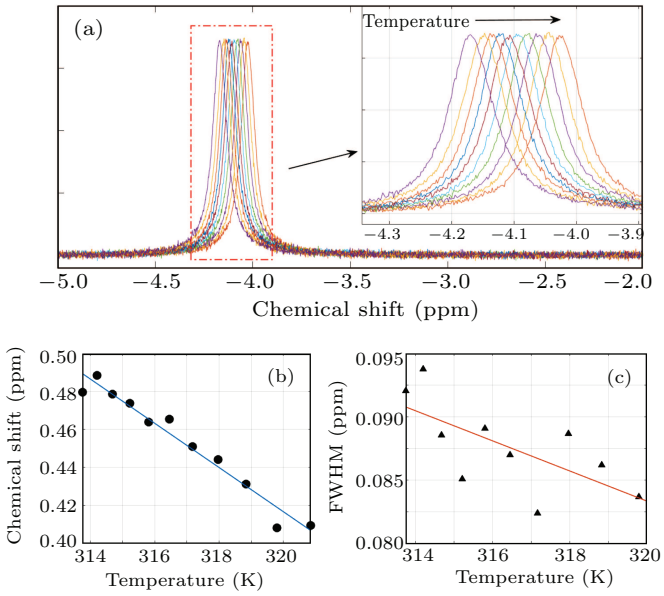


Fig. 8. Temperature-dependent (a) 43-MHz 1-H NMR spectra, (b) chemical shift, and (c) FWHM.

4. Conclusions

In this work, the effect of MNPs on magnetic field homogeneity is studied through simulation and experiments. Based on the spatial distribution of MNPs simulated by Monte Carlo method, the magnetic field uniformity is evaluated by the probability distribution of magnetic field intensity. Both the particle size and concentration of MNPs aggravate the magnetic field inhomogeneity, while the increase of temperature weakens the inhomogeneity. The effect of MNPs on NMR spectrum is explained. The relationship between the properties of MNP reagents and characters of NMR lays a theoretical foundation for improving the performance of temperature imaging and spectral imaging of MNPs.

References

[1] Odeen H and Parker D L 2019 *Prog. Nucl. Magn. Reson. Spectrosc.* **110** 34
[2] VilasBoas-Ribeiro I, Curto S, van Rhoon G C, Franckena M and Paulides M M 2021 *Cancers (Basel)* **13** 3503
[3] Hankiewicz J H, Stoll J A, Stroud J, Davidson J, Livesey K L, Tvrdy K, Roshko A, Russek S E, Stupic K, Bilski P, Camley R E and Celinski Z J 2019 *J. Magn. Magn. Mater.* **469** 550
[4] Hankiewicz J H, Celinski Z, Stupic K F, Anderson N R and Camley R E 2016 *Nat. Commun.* **7** 12415
[5] Zhang Y, Guo S, Zhang P, Zhong J and Liu W 2020 *Nanotechnology* **31** 345101
[6] Guo S, Liu J, Du Z and Liu W 2021 *Rev. Sci. Instrum.* **92** 024901
[7] Rad A M, Arbab A S, Iskander A S, Jiang Q and Soltanian-Zadeh H 2007 *J. Magn. Reson. Imaging* **26** 366
[8] Thorek D L, Chen A K, Czupryna J and Tsourkas A 2006 *Ann. Biomed. Eng.* **34** 23
[9] Huang H S and Hainfeld J F 2013 *Int. J. Nanomedicine* **8** 2521
[10] Hurwitz M and Stauffer P 2014 *Semin. Oncol.* **41** 714
[11] James J R, Gao Y, Miller M A, Babsky A and Bansal N 2009 *Magn. Reson. Med.* **62** 550
[12] Saritas E U, Goodwill P W, Croft L R, Konkle J J, Lu K, Zheng B and Conolly S M 2013 *J. Magn. Reson.* **229** 116
[13] Chen L, Xie J, Wu H, Zang F, Ma M, Hua Z, Gu N and Zhang Y 2018 *Colloids Surf. B Biointerfaces* **161** 339
[14] Rauwerdink A M, Hansen E W and Weaver J B 2009 *Phys. Med. Biol.* **54** L51
[15] Zhong J, Liu W, Du Z, Cesar de Morais P, Xiang Q and Xie Q 2012 *Nanotechnology* **23** 075703
[16] Xu W, Liu W and Zhang P 2016 *Rev. Sci. Instrum.* **87** 054902
[17] Zhong J, Schilling M and Ludwig F 2018 *Measurement Science and Technology* **29** 115903
[18] Zhong J, Liu W, Kong L and Morais P C 2014 *Sci. Rep.* **4** 6338
[19] Weaver J B, Rauwerdink A M and Hansen E W 2009 *Med. Phys.* **36** 1822
[20] Brown R J S 1961 *Phys. Rev.* **121** 1379
[21] Seleznyova K, Strugatsky M and Kliava J 2016 *Eur. J. Phys.* **37** 025203
[22] Ando T, Hirota N and Wada H 2009 *Sci. Technol. Adv. Mater.* **10** 014609
[23] Dirac P A M 1948 *Phys. Rev.* **74** 817
[24] Ivanov A O and Kuznetsova O B 2001 *Phys. Rev. E* **64** 041405
[25] Vuong Q L, Gillis P and Gossuin Y 2011 *J. Magn. Reson.* **212** 139
[26] van der Waals J D 1979 *Journal of Statistical Physics* **20** 200
[27] Satoh A, Chantrell R W, Kamiyama S I and Coverdale G N 1996 *J. Colloid Interf. Sci.* **178** 620
[28] Chen Y H, Guo X R, Du X L and Guo G L 2002 *Acta Phys. Chim. Sin.* **18** 710
[29] Keevil S F 2006 *Phys. Med. Biol.* **51** R579
[30] Hardy R C and Cottington R L 1949 *Journal of Research of the National Bureau of Standards* **42** 573
[31] Cini R and Torrini M 1968 *J. Chem. Phys.* **49** 2826